Ceramics International 46 (2020) 15665–15669

Contents lists available at ScienceDirect

Ceramics International

journal homepage: www.elsevier.com/locate/ceramint

# The effects of $TiO_2$ addition on microwave dielectric properties of $Y_3MgAl_3SiO_{12}$ ceramic for 5G application

Zhenyu Tan[a], Kaixin Song[a,*], Hadi Barzegar Bafrooei[a,c], Bing Liu[a], Jun Wu[a], Junming Xu[a], Huixing Lin[b], Dawei Wang[d,**]

[a] College of Electronics Information, Hangzhou Dianzi University, Hangzhou, 310018, China
[b] Key Laboratory of Inorganic Functional Material and Device, Shanghai Institute of Ceramics, Chinese Academy of Sciences, Shanghai, 200050, China
[c] Department of Materials Science and Engineering, School of Engineering, Meybod University, Yazd, Iran
[d] Department of Materials Science and Engineering, The University of Sheffield, Sheffield, S1 3JD, UK

ARTICLE INFO

*Keywords:*
Microwave dielectric properties
Microstructure
Yttrium aluminum garnet

ABSTRACT

In this paper, thermal stable $Y_3MgAl_3SibO_{12}$-$TiO_2$ microwave composite ceramics were firstly fabricated by the high temperature solid phase reaction method. The influence of the sintering temperature, microstructure on microwave dielectric properties of $Y_3MgAl_3SiO_{12}$ by doping $TiO_2$ were investigated in detailed. $TiO_2$ addition reduced the ceramic sintering temperature and improved the distribution of grain size. The negative temperature coefficient of resonant frequency ($\tau_f$ = −32 ppm/°C) of $Y_3MgAl_3SiO_{12}$ was adjusted to near zero value. $0.8Y_3MgAl_3SiO_{12}$-$0.2TiO_2$ ceramic sintered at 1475 °C for 6 h achieved the optimized microwave dielectric properties: $\varepsilon_r$ = 12.2, Q × f = 21,050 GHz, $\tau_f$ = +5.2 ppm/°C, which indicated that $0.8Y_3MgAl_3SiO_{12}$-$0.2TiO_2$ is a potential candidate for dielectric patch antenna and substrate.

## 1. Introduction

With the development of the Internet of Things, Internet+, 5G Communication, and Multi-Channel Communication Technologies, new communication technologies require faster transmission speed and higher quality of signals, leading to urgent development of novel microwave dielectric ceramic materials [1–3]. Especially, ceramic materials with low dielectric constant ($\varepsilon_r$ < 15), and higher quality factor (Q × f > 10000 GHz) and near-zero temperature coefficient of resonant frequency ($\tau_f$ = ± 10 ppm/°C) are the hotspots of research. Silicate ceramics and composites, including willemite [4], pyroxene [5], cordierite [6], $Mg_2SiO_4$–$CaTiO_3$ [7] and mullite-SiC [8], are a series of important and promising microwave dielectric ceramics for 5G communication. Song et al. firstly reported the microwave dielectric properties of pure phase garnet type $Y_3MgAl_3SiO_{12}$ ceramic with $\varepsilon_r$ = 10.1, Q × f = 57,340 GHz, $\tau_f$ = −32 ppm/°C [9]. However, the $\tau_f$ of $Y_3MgAl_3SiO_{12}$ is negative, not near zero. The $\tau_f$ value of willemite and cordierite had been reported to tune to zero by the addition of $TiO_2$ with positive $\tau_f$ (+460 ppm/°C) [10,11]. However, most silicate ceramics were difficult to tune $\tau_f$ to zero by the either mixing end-members with negative and positive $\tau_f$ or formation of solid solution by high temperature solid state reaction, like forsterite and mullite ceramics [12–14]. Herein, in order to tune $\tau_f$ of $Y_3MgAl_3SiO_{12}$ to near zero, $TiO_2$ with positive $\tau_f$ was selected to form new composite ceramics. The microstructure microwave dielectric properties of $Y_3MgAl_3SiO_{12}$–$TiO_2$ were studied as a function of sintering temperature and $TiO_2$ amount.

## 2. Experimental procedure

$(1\text{-}x)Y_3MgAl_3SiO_{12}$-$x TiO_2$ ($x$ = 0, 0.05, 0.10, 0.15, 0.20, abbreviated as $YMAST_{00}$, $YMAST_{05}$, $YMAST_{10}$, $YMAST_{15}$ and $YMAST_{20}$) ceramics were prepared by traditional solid state reaction method. High purity raw materials MgO (4 N, Aladdin Industrial Corporation), $Y_2O_3$ (4 N, Aladdin Industrial Corporation), $Al_2O_3$ (4 N, Aladdin Industrial Corporation) and $SiO_2$ (4 N, Aladdin Industrial Corporation) were weighted and calcined at 1300 °C for 4 h. After adding different molar ratios of $TiO_2$ (99.00%) in $Y_3MgAl_3SiO_{12}$, then the mixtures were ground by a planetary ball mill for 1 h and then dried at 120 °C. Subsequently, the powders were pressed into cylindrical green bodies (Φ15 mm × 8 mm). Finally, the green pellets were sintered at 1425–1625 °C for 6 h at a heating rate of 4 °C/min.

The bulk densities of sintered ceramic samples were measured by the Archimedes method. The crystalline phases of the ceramics were identified by X-ray diffraction (XRD) using Cu Kα radiation with Ultima

* Corresponding author.,
** Corresponding author.
*E-mail addresses:* kxsong@hdu.edu.cn (K. Song), dawei.wang@sheffield.ac.uk (D. Wang).

https://doi.org/10.1016/j.ceramint.2020.03.116
Received 13 February 2020; Received in revised form 28 February 2020; Accepted 10 March 2020
Available online 16 March 2020
0272-8842/ 

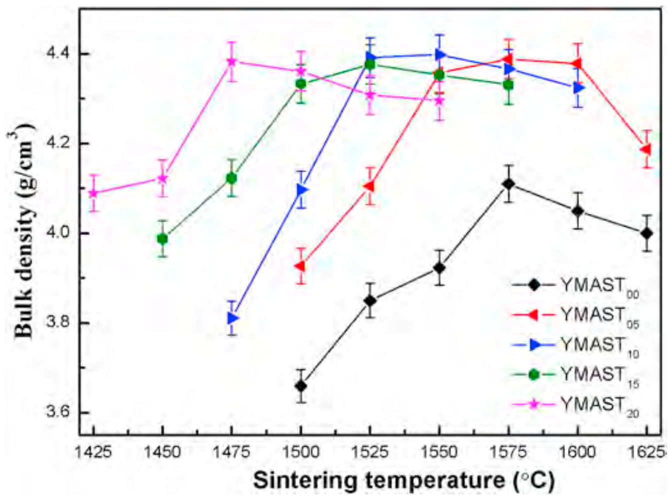


**Fig. 1.** The bulk density of $YMAST_{00}$, $YMAST_{05}$, $YMAST_{10}$, $YMAST_{15}$ and $YMAST_{20}$ ceramics sintered for 6 h

IV (Rigaku, Japan) operated at 40 kV and 40 mA. The morphology of ceramics was examined using a scanning electron microscopy (SEM, Hitachi S-4800, Hitachi, Japan). The dielectric properties of the samples were measured by Agilent E5071C network analyzer. The $\tau_f$ was calculated with the following formula:

$$\tau_f = \frac{(f_2 - f_1) \times 10^6}{f_1(T_2 - T_1)} \text{ (ppm/°C)} \quad (1)$$

Where $f_2$ and $f_1$ represent the resonant frequency at $T_2$ and $T_1$, respectively. $T_1$ and $T_2$ are 85 °C and 25 °C, respectively [15].

## 3. Results and discussion

Fig. 1 showed the relationship between bulk density and sintering temperature of $YMAST_{00}$, $YMAST_{05}$, $YMAST_{10}$, $YMAST_{15}$ and $YMAST_{20}$ ceramics. The bulk density of all ceramics increased with increasing temperature and then decreased after reaching the maximum values, which indicated that there was an optimum densification temperature as listed in Table .1. On the other hand, it should be noted that the densification temperature of ceramics with adding $TiO_2$ was lower than the sample without $TiO_2$ adding. With the increase of $TiO_2$ content, the sintering temperature was found to decrease and the sintering range was broadened, indicating $TiO_2$ was beneficial for reducing sintering temperature and densification of ceramics.

XRD patterns of $YMAST_{00}$, $YMAST_{05}$, $YMAST_{10}$, $YMAST_{15}$ and $YMAST_{20}$ ceramics at the optimum sintering temperature were showed in Fig. 2. The diffraction peak of $YMAST_{00}$ matched well with the standard PDF card of $Al_5Y_3O_{12}$ (Cubic Crystal System, Space Group *la-3d*), it was a single-phase. With the increase of $TiO_2$ content, impurities $Y_2Ti_2O_7$ (PDF#28–2065) and $TiO_2$ (PDF#99–0008) were found in the samples and the intensity of the diffraction peak gradually increased. Combining theoretical balance formulas and XRD, we can know that part of $TiO_2$ chemically reacted with $Y_3MgAl_3SiO_{12}$ to form $Y_2Ti_2O_7$ [16] and glass phase.

The SEM images of (1-*x*) $Y_3MgAl_3SiO_{12}$-$xTiO_2$ ceramics were given in Fig. 3(a–d), where we can see that the grain sizes distribution was uniform and the grain sizes tended to decrease with increasing $TiO_2$ amount, Grain size distribution was obtained by Image J and Gaussian Fitting, as displayed in Fig. 3(e–h). The average grain size decreased slightly from 2.1 μm for $YMAST_{05}$ and $YMAST_{10}$ to 1.9 μm for $YMAST_{15}$ and $YMAST_{20}$ with the amount of $TiO_2$ increased, because $TiO_2$ and Rod-shaped grains seated at the grain boundary and pores, and inhibited the grain growth. Fig. 4 was the EDS of $YMST_{20}$ ceramic at 1475 °C. The content of Magnesium and Silicon were basically unchanged, point B has higher content of Oxygen and Titanium, lower content of Aluminum, which can be indicative of the $Y_2Ti_2O_7$ phase in Rod-shaped grains, in agreement with the XRD data (Fig. 2).

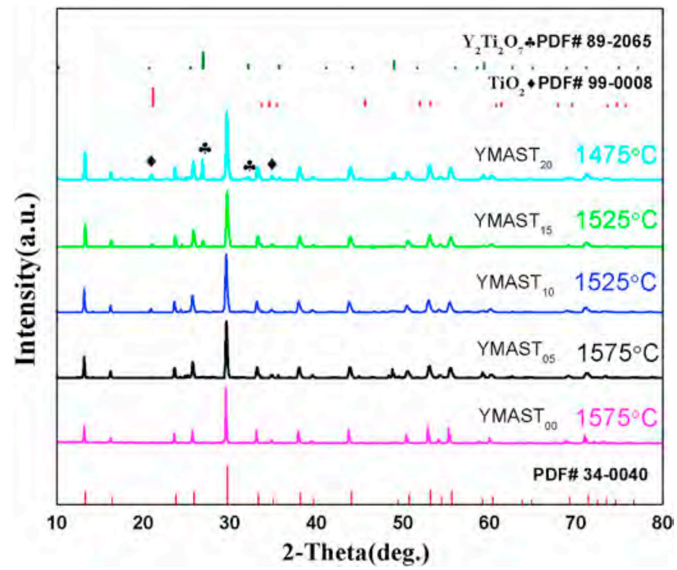


**Fig. 2.** The XRD of $YMAST_{00}$, $YMAST_{05}$, $YMAST_{10}$, $YMAST_{15}$ and $YMAST_{20}$ ceramics at the optimum temperature for 6 h

The relative dielectric constant ($\varepsilon_r$) of $YMAST_{05}$, $YMAST_{10}$, $YMAST_{15}$ and $YMAST_{20}$ as a function of sintering temperature was shown in Fig. 5. The $\varepsilon_r$ appeared to increase rapidly with the increase of sintering temperature at first, and then tended to be stable, agreeing well with the change of bulk density (Fig. 1). Furthermore, $\varepsilon_r$ value increased with the increase of $TiO_2$ amount in Fig. 5, attributed to the much higher $\varepsilon_r$ value of $TiO_2$ (~106) than that of $Y_3MgAl_3SiO_{12}$ (~10) [17]. According to the mixing law, the $\varepsilon_r$ of composites should meet the following formula [18–21]:

$$\ln\varepsilon = X_Y \ln\varepsilon_Y + X_T \ln\varepsilon_T \quad (2)$$

Where $X_Y$ and $X_T$ are the percentage of $Y_3MgAl_3SiO_{12}$ and $TiO_2$ in the total volume, respectively. $\varepsilon_Y$ and $\varepsilon_T$ are the $\varepsilon_r$ of $Y_3MgAl_3SiO_{12}$ and $TiO_2$, respectively. Since the $\varepsilon_r$ value of $TiO_2$ (~106) is much larger than of $Y_3MgAl_3SiO_{12}$, the overall $\varepsilon_r$ increased with the increase of $TiO_2$. It demonstrated that the addition of $TiO_2$ was useful to improve $\varepsilon_r$ value of $Y_3MgAl_3SiO_{12}$ ceramics.

Fig. 6 showed the Q × *f* of (1-*x*) $Y_3MgAl_3SiO_{12}$-$xTiO_2$ ceramics increased at first and then decreased after reaching the optimum value with the increase of sintering temperature, indicating that Q × *f* value was closely related to bulk density. It is well-known that the dielectric loss is mainly composed of intrinsic loss and extrinsic loss. Intrinsic loss is mainly affected by internal factors such as ionic polarization and crystal structure. The extrinsic loss is mainly affected by external

**Table 1**
The optimal sintering temperature and optimal bulk density of $YMAST_{00}$, $YMAST_{05}$, $YMAST_{10}$, $YMAST_{15}$ and $YMAST_{20}$.

| | $YMAST_{00}$ | $YMAST_{05}$ | $YMAST_{10}$ | $YMAST_{15}$ | $YMAST_{20}$ |
|---|---|---|---|---|---|
| Optimal sintering temperature | 1575 °C | 1575 °C | 1525 °C | 1525 °C | 1475 °C |
| Optimal bulk density | 4.110 g/cm$^3$ | 4.388 g/cm$^3$ | 4.389 g/cm$^3$ | 4.379 g/cm$^3$ | 4.382 g/cm$^3$ |

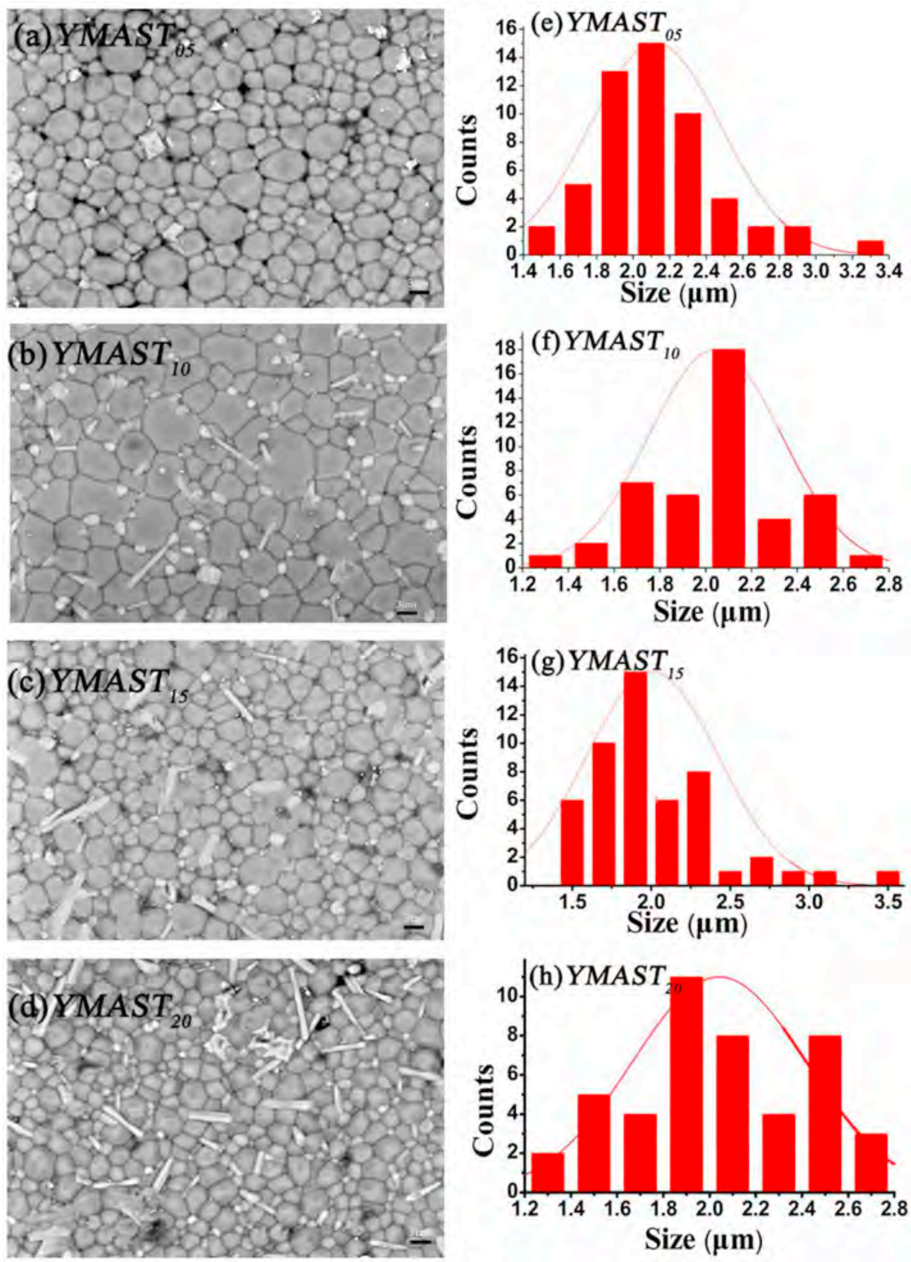


**Fig. 3.** The SEM and grain size distribution of $YMAST_{05}$, $YMAST_{10}$, $YMAST_{15}$ and $YMAST_{20}$ ceramics at optimum sintering temperature.

defects such as second phase, grain size and distribution, grain boundaries, glass phase and oxygen vacancies. The Q × *f* of $YMAST_{05}$ and $YMAST_{10}$ ceramics were smaller than that of pristine samples, mainly because a small amount of secondary phase had little effect on the Q × *f* value of $Y_3MgAl_3SiO_{12}$ ceramics. With the increase of $TiO_2$, the decreasing trend of *Q* × *f* became faster, indicating that excessive $TiO_2$ incorporation caused lattice defects. When x ≥ 0.2, Q × *f* decreased further from about 54,000 GHz to about 21,000 GHz, which was mainly related to the second phase of glass phase, $TiO_2$ and $Y_2Ti_2O_7$, whose Q × *f* only is 9,000 GHz [22]. Herein, the secondary phases were the main cause of the sharp deterioration of the Q × *f* value of YMAST ceramics. Although the second phase filled some of the pores and limited the growth of grains, the second phase led to an increase in the grain boundary of $Y_3MgAl_3SiO_{12}$, which were easy to produce the internal stress of lattice distortion to increase, causing an increase in loss.

The $\varepsilon_r$, Q × *f and* $\tau_f$ of (1-*x*) $Y_3MgAl_3SiO_{12}$-$x TiO_2$ ceramics as a function of x value sintered at the optimum temperature were shown in Fig. 7. The red line displayed that $\varepsilon_r$ value of all ceramic samples with $TiO_2$ was increased compared with $\varepsilon_r$ value of ceramic sample without $TiO_2$, *Q* × *f* had the opposite trend compared with $\varepsilon_r$ value as showed with black line, all in agreement with the theoretical explanations. The blue line in Fig. 7 was obvious that the $\tau_f$ value increased from −25.3 ppm/°C to 5.23 ppm/°C, being consistent with the calculation theory of the composite ceramic, described in the following formula [18–21]:

$$\tau f = V_1 \tau f_1 + V_2 \tau f_2 + V_3 \tau f_3 \tag{3}$$

Where $V_1$, $V_2$ and $V_3$ are respectively the percentage of $TiO_2$, $Y_2Ti_2O_7$ and $Y_3MgAl_3SiO_{12}$ in the total volume, $\tau_{f1}$, $\tau_{f2}$ and $\tau_{f3}$ are the $\tau_f$ value $TiO_2$, $Y_2Ti_2O_7$ and $Y_3MgAl_3SiO_{12}$ [23]. The $\tau_f$ of $TiO_2$ is +460 ppm/°C, the $\tau_f$ of $Y_2Ti_2O_7$ is −30 ppm/°C and the $\tau_f$ of $Y_3MgAl_3SiO_{12}$ is −28.1 ppm/°C. Therefore, the $\tau_f$ value of (1-*x*) $Y_3MgAl_3SiO_{12}$-$x TiO_2$ ceramic was closer to zero with the increase of $TiO_2$.

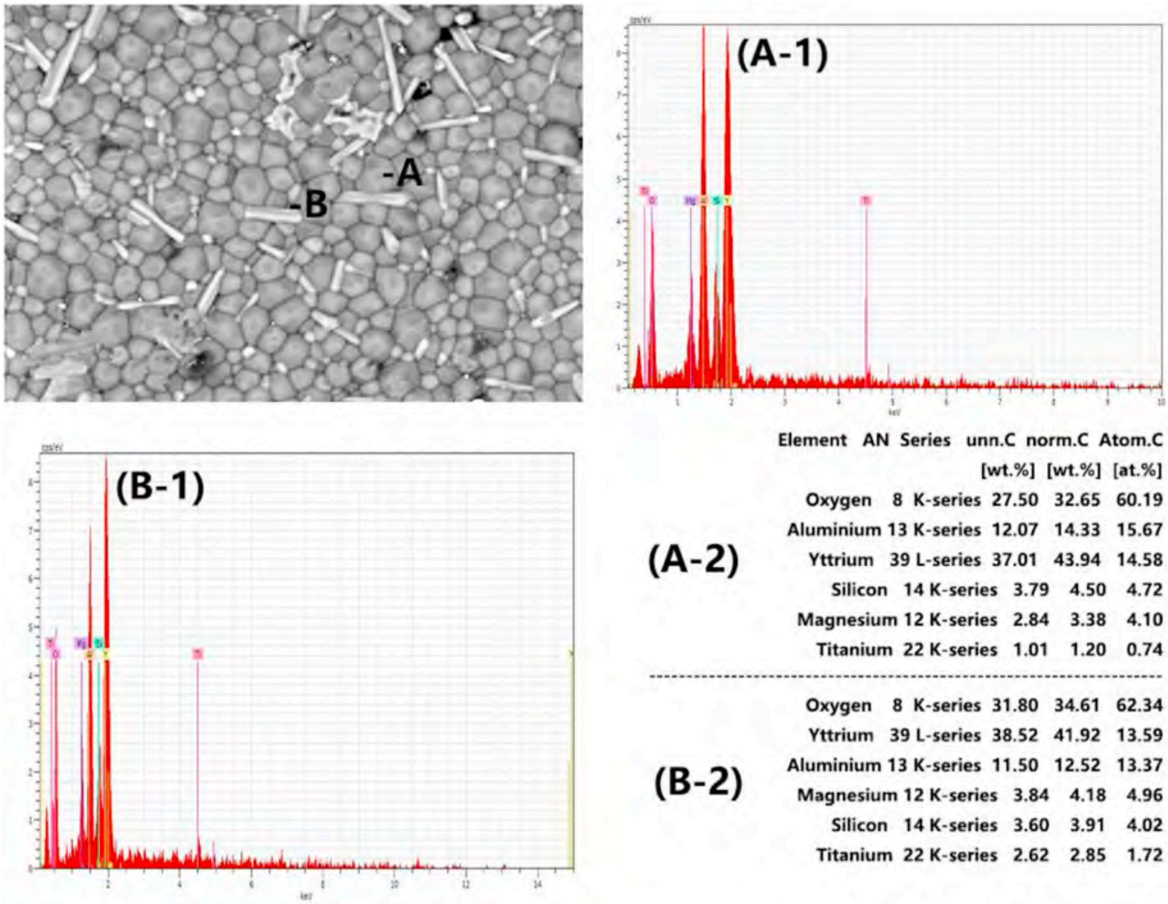


**Fig. 4.** The EDS of $YMAST_{20}$ ceramic at optimum sintering temperature.

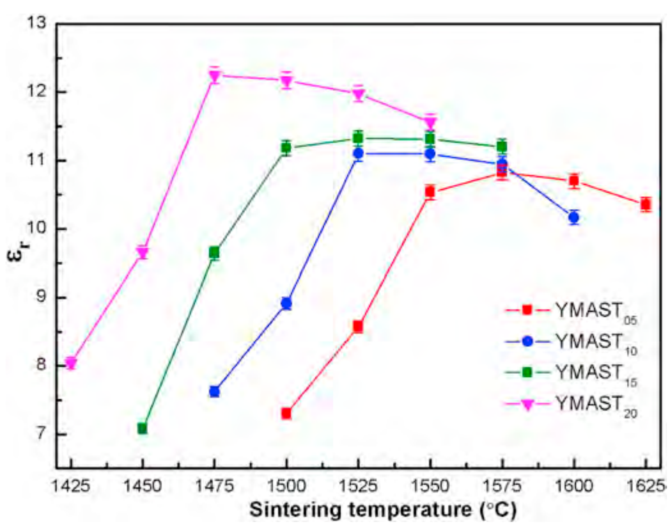


**Fig. 5.** The $\varepsilon_r$ of $YMAST_{05}$, $YMAST_{10}$, $YMAST_{15}$ and $YMAST_{20}$ ceramics sintered for 6 h.

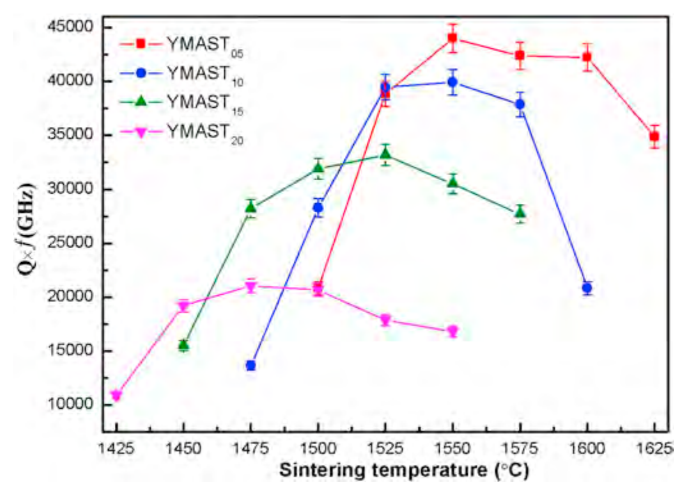


**Fig. 6.** The Q × f of $YMAST_{05}$, $YMAST_{10}$, $YMAST_{15}$ and $YMAST_{20}$ ceramics sintered for 6 h.

## 4. Conclusions

(1-x)$Y_3MgAl_3SiO_{12}$-x$TiO_2$ composite ceramics were prepared by a high temperature solid phase reaction method. $TiO_2$ addition reduced and broadened the sintering temperature and range of the composite ceramics. The XRD patterns showed that with the addition of $TiO_2$, the main crystalline phase was still $Y_3MgAl_3SiO_{12}$, and the second phases of $Y_2Ti_2O_7$ and $TiO_2$ appeared. With the amount of $TiO_2$ increased, the densification temperature and $Q \times f$ was lowered, and the $\varepsilon_r$ and $\tau_f$ increased. The optimized microwave dielectric properties of $YMAST_{05}$ ceramic sintered at 1550 °C was achieved: $\varepsilon_r$ = 10.7, $Q\times f$ = 42,242 GHz, $\tau_f$ = −25.40 ppm/°C. $YMAST_{10}$ ceramic $YMAST_{05}$ ceramic showed the optimized microwave dielectric properties sintered at 1525 °C: $\varepsilon_r$ = 11.0, $Q\times f$ = 39,929 GHz, $\tau_f$ = −20.16 ppm/°C. $YMAST_{15}$ ceramic achieved the optimized microwave dielectric properties at 1525 °C: $\varepsilon_r$ = 11.3, $Q\times f$ = 31,195 GHz, $\tau_f$ = −10.69 ppm/°C. $YMAST_{20}$ ceramic achieved the optimized microwave dielectric properties at 1475 °C: $\varepsilon_r$ = 12.2, Q × $f$ = 21,050 GHz, $\tau_f$ = +5.2 ppm/°C.

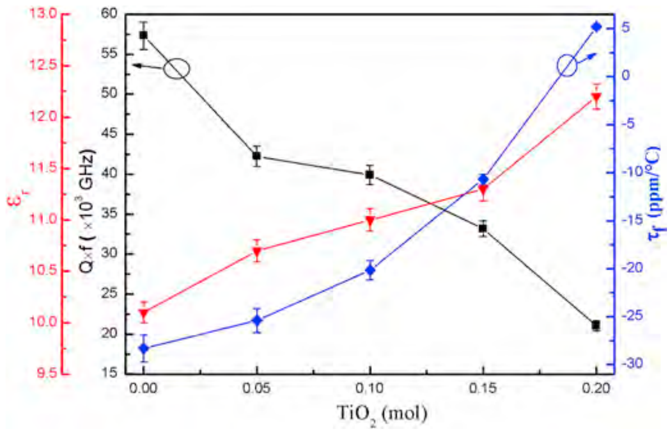


**Fig. 7.** The $\varepsilon_r$, Q × *f and* $\tau_f$ of (1-*x*) $Y_3MgAl_3SiO_{12}$-*x*$TiO_2$ ceramics sintered at the optimum temperature for 6 h as a function of x value.

## Declaration of competing interest

The authors declare that they have no known competing financial interests or personal relationships That could have appeared to influence the work reported in this paper.

## Acknowledge

This work was supported by the National Natural Science Foundation of China under grant number 51672063 and 51802062, Cultivation plan of young and middle-aged academic leaders in Zhejiang Province under grant number: GK188800207036, GK1988002099407-002. Open projects of Key Laboratory of inorganic functional materials and devices, Shanghai silicate institutes, Chinese academy of sciences under grant number: KLIFMD201708.

## References


[1] Z.X. Fang, Bin Tang, Temperature stable and high-Q microwave dielectric ceramics in the $Li_2Mg_{3-x}Ca_xTiO_6$ system (x = 0.00–0.18) [J], Ceram. Int. 2 (2017) 1682–1687.
[2] X.K. Lan, Lei Wen, Lattice structure and microwave dielectric properties of $[Mg_{0.5}Si_{0.5}]^{3+}$-doped $LiAlO_2$ solid solution [J], J. Mater. Sci. Mater. Electron. 30 (2019) 11764–11770.
[3] J. Li, Lei Wen, Ultra broad temperature stability of stuffed tridymite-type $BaAl_2O_4$ co-doped by $[Zn_{0.5}Ti_{0.5}]^{3+}$ with weak Ferro electricity [J], Ceram. Int. 45 (2019) 22493–22497.
[4] Z.H. Zhou, X.L. Tang, Microwave dielectric properties of LBBS glass added $(Zn_{0.95}Co_{0.05})_2SiO_4$ for LTCC technology [J], Ceram. Int. 42 (2016) 11161–11164.
[5] H. Sun, J. Zou, $(Ca_{1-x}Mgx)SiO_3$: a low-permittivity microwave dielectric ceramic system [J], Mater. Adv. Technol. 138 (2007) 46–50.
[6] J.S. Wei, K.X. Song, Crystal structure and microwave dielectric properties of $CaTiO_3$ modified $Mg_2Al_4Si_5O_{18}$ cordierite ceramics [J], J. Alloys Compd. 689 (2016) 81–86.
[7] G. Dou, M. Guo, Low-temperature sintered $Mg_2SiO_4$-$CaTiO_3$ ceramics with near-zero temperature coefficient of resonant frequency [J], J. Mater. Sci. Mater. Electron. 24 (2013) 1431–1438.
[8] Hui Gao, Fa Luo, Effect of preparation conditions on mechanical, dielectric and microwave absorption properties of SiC fiber/mullite matrix composite [J], Ceram. Int. 45 (2019) 11625–11632.
[9] J.B. Song, K.X. Song, Ionic occupation, structures and microwave dielectric properties of $Y_3MgAl_3SiO_{12}$ garnet-type ceramics [J], J. Am. Ceram. Soc. 101 (2018) 244–251.
[10] Z.Z. Weng, C.X. Song, Microstructure and broadband dielectric properties of $Zn_2SiO_4$ ceramics with nano-sized $TiO_2$ addition [J], Ceram. Int. 45 (2019) 13251–13256.
[11] S. Wu, K.X. Song, Effect of $TiO_2$ doping on the structure and microwave dielectric properties of cordierite ceramics [J], J. Am. Ceram. Soc. 98 (2015) 1842–1847.
[12] T. Tsunooka, Y. Higashida, Effects of $TiO_2$ on sinter ability and dielectric properties of high-Q forsterite ceramics [J], J. Eur. Ceram. Soc. 23 (2003) 2573–2578.
[13] B. Zhang, et al., Ultra-low cost porous mullite ceramics with excellent dielectric properties and low thermal conductivity fabricated from kaolin for radome applications [J], Ceram. Int. 45 (2019) 18865–18870.
[14] J. Wang, et al., The microstructure, mechanical and dielectric properties of CNTs/mullite ceramics composite [J], Key Eng. Mater. 313 (2006) 145–150.
[15] K.X. Song, Z.H. Ying, Phase evolution and microwave dielectric properties in the systems of $(Mg_{1-x}Ca_x)_2SiO_4$ ceramics [J], Adv. Mater. Res. 152 (2010) 801–804.
[16] X.J. Wang, X.J. Mao, Fabrication and properties of $Y_2Ti_2O_7$ transparent ceramics with excess Y content [J], Ceram. Int. 44 (2018) 9514–9518.
[17] J. Guo, D. Zhou, Microwave dielectric properties of (1 − x) $ZnMoO_4$–x$TiO_2$ composite ceramics [J], J. Alloys Compd. 509 (2011) 5863–5865.
[18] Z.X. Fang, Bin Tang, Temperature stable and high-Q microwave dielectric ceramics in the $Li_2Mg_{3-x}Ca_xTiO_6$ system (x = 0.00–0.18) [J], Ceram. Int. 43 (2017) 1682–1687.
[19] D. Wang, S. Zhang, G. Wang, Y. Vardaxoglou, W. Whittow, D. Cadman, D. Zhou, K. Song, I. M Reaney, Cold sintered $CaTiO_3$-$K_2MoO_4$ microwave dielectric ceramics for integrated microstrip patch antennas [J], Applied Materials Today 18 (2020) 100519.
[20] D. Wang, S. Zhang, D. Zhou, K. Song, A. Feteira, Y. Vardaxoglou, W. Whittow, D. Cadman, I.M. Reaney, Temperature stable cold sintered $(Bi_{0.95}Li_{0.05})(V_{0.9}Mo_{0.1})O_4$-$Na_2Mo_2O_7$ microwave dielectric composites[J], Materials 12 (2019) 1370 (Invited feature article).
[21] D. Wang, D. Zhou, S. Zhang, Y. Vardaxoglou, W.G. Whittow, D. Cadman, I.M. Reaney, Cold-sintered temperature stable $Na_{0.5}Bi_{0.5}MoO_4$-$Li_2MoO_4$ microwave composite ceramics[J], ACS Sustain. Chem. Eng. 6 (2018) 2438–2444.
[22] Y. Xiao, Q.T. Zhang, Microwave dielectric properties of $(Y_{0.99}R_{0.01})_2Ti_2O_7$(R = Pr, Tb, Ho, Er, Tm, Yb, Lu) [J], Functional Materials 42 (2011) 762–765.
[23] S.X. Duan, Bin Tang, Influence of $Li_2O$–$B_2O_3$–$SiO_2$ glass on the sintering behavior and microwave dielectric properties of BaO–0.15ZnO–4$TiO_2$ ceramics [J], Ceram. Int. 42 (2016) 7943–7949.